



Published in final edited form as:

*Biochemistry*. 2012 November 13; 51(45): 9245–9255. doi:10.1021/bi3006829.

## Pseudouridine Monophosphate Glycosidase: a New Glycosidase Mechanism<sup>†,‡</sup>

Siyu Huang<sup>a</sup>, Nilkamal Mahanta<sup>b</sup>, Tadhg P. Begley<sup>b,\*</sup>, and Steven E. Ealick<sup>a,\*</sup>

<sup>a</sup>Department of Chemistry and Chemical Biology, Cornell University, Ithaca, New York 14853, USA

<sup>b</sup>Department of Chemistry, Texas A&M University, College Station, Texas 77843, USA

### Abstract

Pseudouridine ( $\Psi$ ), the most abundant modification in RNA, is synthesized *in situ* using  $\Psi$  synthase. Recently, a pathway for the degradation of  $\Psi$  was described. In this pathway  $\Psi$  is first converted to  $\Psi$  5'-monophosphate ( $\Psi$ MP) by  $\Psi$  kinase and then  $\Psi$ MP is degraded by  $\Psi$ MP glycosidase to uracil and ribose 5-phosphate.  $\Psi$ MP glycosidase is the first example of a mechanistically-characterized enzyme that cleaves a C-C glycosidic bond. Here we report X-ray crystal structures of *Escherichia coli*  $\Psi$ MP glycosidase and a complex of the K166A mutant with  $\Psi$ MP. We also report the structures of a ring-opened ribose 5-phosphate adduct and a ring-opened ribose  $\Psi$ MP adduct. These structures provide four snapshots along the reaction coordinate. The structural studies suggested that the reaction utilizes a Lys166 adduct during catalysis. Biochemical and mass spectrometry data further confirmed the existence of a lysine adduct. We used site directed mutagenesis combined with kinetic analysis to identify roles for specific active site residues. Together, these data suggest that  $\Psi$ MP glycosidase catalyzes the cleavage of the C-C glycosidic bond through a novel ribose ring-opening mechanism.

Pseudouridine ( $\Psi$ ) was the first modified nucleoside to be discovered and is the most abundant modification in RNA, existing in tRNAs, rRNAs, snRNAs and snoRNAs (1).  $\Psi$  is biosynthesized post-transcriptionally from RNA uridine moieties by  $\Psi$  synthase, which cleaves the glycosidic C-N bond and reconnects the uracil to the ribosyl moiety at the C5 position (2). Pseudouridine reduces the conformational flexibility of RNA because the exposed, protonated N1 atom forms strong hydrogen bonds with structured water molecules, replacing weak interactions formed by C5 (1, 3).

While  $\Psi$  biosynthesis has been studied extensively, little is known about  $\Psi$  catabolism. Recently, the two enzymes responsible for  $\Psi$  1 degradation in *Escherichia coli* were identified (4).  $\Psi$  kinase first phosphorylates  $\Psi$  to pseudouridine 5'-phosphate ( $\Psi$ MP, 2).

<sup>†</sup>This work was supported by NIH grant GM73220 (to SEE) and by the Robert A. Welch Foundation (A-0034 to TPB). This work is based upon research conducted at the Advanced Photon Source on the Northeastern Collaborative Access Team beamlines, which are supported by award GM103403 from the National Institute of General Medical Sciences at the National Institutes of Health. Use of the Advanced Photon Source is supported by the U.S. Department of Energy, Office of Basic Energy Sciences, under Contract No. DE-AC02-06CH11357. MacCHESS is supported by NIH grant RR01646 at the Cornell High Energy Synchrotron Source.

<sup>‡</sup>The Protein Data Bank codes have been deposited under the accession number 4GIJ, 4GIK, 4GIL and 4GIM for  $\Psi$ MP glycosidase, the R5P adduct, the  $\Psi$ MP covalent adduct, and the K166A/ $\Psi$ MP complex, respectively.

<sup>\*</sup>To whom correspondence should be addressed at the Department of Chemistry and Chemical Biology, Cornell University, Ithaca, NY 14853. Telephone: (607) 255-7961. Fax: (607) 255-1227. see3@cornell.edu, begley@mail.chem.tamu.edu.

#### SUPPORTING INFORMATION AVAILABLE

Supplementary material includes Supplementary Figure 1, which consists of the Michaelis-Menten plots for  $\Psi$ MP glycosidase and mutants, and Supplementary Table 1, which shows the primers used for the mutations. This material is available free of charge via the Internet at <http://pubs.acs.org>.

$\Psi$ MP glycosidase then catalyzes the reversible cleavage of the C-C glycosidic bond to form uracil **4** and ribose 5-phosphate (R5P, **3**) (Scheme 1). While  $\Psi$ MP glycosidase functions biologically in the cleavage direction, equilibrium strongly favors  $\Psi$ MP synthesis with an equilibrium constant for the degradation reaction of  $2.3 \times 10^{-4}$  M (**4**). In bacterial genomes  $\Psi$  kinase and  $\Psi$ MP glycosidase are encoded by separate genes. In *E. coli* these genes are *yeiC* and *yeiN*, respectively, which are located in the same operon. In some eukaryotes, the genes for  $\Psi$  kinase and  $\Psi$ MP glycosidase are fused, resulting in a bifunctional enzyme. Enzymes metabolizing  $\Psi$  are not found in humans and most other higher organisms, and excess  $\Psi$  is excreted (**5**).

While natural products containing O and N glycosidic bonds are widespread, natural products containing the C-glycosidic bond are much less prevalent (**6**). The C-glycosidic bond is generally assumed to be formed by an electrophilic aromatic substitution. Enzymes that cleave C-N glycosidic bonds have been extensively studied. These include nucleoside and nucleotide hydrolases (**7-9**), purine and pyrimidine nucleoside phosphorylases (**10**), purine and pyrimidine phosphoribosyltransferases (**11, 12**), and nucleoside deoxyribosyltransferases (**13**). In addition, DNA-repair enzymes such as endonuclease III function as N-glycosylases to excise damaged nucleobases from DNA (**14**). Enzymes that cleave C-O glycosidic bonds are widespread in carbohydrate metabolism and have also been extensively studied (**15**). Biochemical, biophysical and genetic studies suggest that these enzymes cleave C-N and C-O glycosidic bonds by a largely dissociative mechanism generating an oxocarbenium ion intermediate. While the genes encoding several C-glycosynthases have been identified and in many cases overexpressed (**16-23**) – and the structures of ligand free UrdGT2 (**24, 25**) and  $\Psi$ MP glycosidase (**26**) have been determined – there is currently no example of a mechanistically well-characterized C-glycosidase or glycosynthase.

Here we report a set of *E. coli*  $\Psi$ MP glycosidase (Ec $\Psi$ MP glycosidase) crystal structures, which provide four snapshots of the reaction coordinate. The structures are: the unliganded enzyme, a  $\Psi$ MP glycosidase/ring-opened R5P adduct, a  $\Psi$ MP glycosidase/ ring-opened ribose  $\Psi$ MP adduct, and a K166A  $\Psi$ MP complex. The structural studies suggested that the reaction involves an intermediate imine with Lys166. This was confirmed by mass spectrometry. Kinetic studies on active site mutants suggested roles for individual amino acid side chains. Comparison of the Ec $\Psi$ MP glycosidase structures suggested a role for conformational changes in  $\Psi$ MP cleavage and product release. These results suggest an unanticipated mechanism for the pseudouridine glycosidase catalyzed C-glycosyl bond hydrolysis.

## MATERIAL AND METHODS

### Chemical Reagents

R5P and uracil were purchased from Sigma-Aldrich. Tris(2-carboxyethyl)phosphine (TCEP) was purchased from Hampton Research. Kanamycin was purchased from Acros. Ni-NTA resin was obtained from Qiagen (Valencia, CA).

### Cloning, Overexpression and Purification of $\Psi$ MP Glycosidase

Standard methods were used for DNA restriction endonuclease digestion, ligation and transformation of DNA (**27**). Automated DNA sequencing was performed at the Cornell BioResource Center. Plasmid DNA was purified with a GeneJet miniprep kit (Fermentas, Glen Burnei, MD). DNA fragments were separated by agarose gel electrophoresis, excised and purified with the Zymoclean gel DNA recovery kit (Zymo Research, Orange, CA). *E. coli* strain MachI (Invitrogen, Madison, WI) was used as the recipient for transformations

during plasmid construction and for plasmid propagation and storage. An Eppendorf Mastercycler and Phusion DNA polymerase (New England Biolabs, Ipswich, MA) were used for PCR. All restriction endonucleases and T4 DNA ligase were purchased from New England Biolabs (Ipswich, MA). *E. coli* strain BL21(DE3) and the pET overexpression system were purchased from Novagen (Madison, WI).

The *yeiN* gene was PCR amplified from *E. coli* K12 genomic DNA using the following primers: upstream primer 5'-GGG TAG CAT ATG TCT GAA TTA AAA ATT TCC CCT G-3' (inserts an *NdeI* site at the start codon of the *yeiN* open reading frame); downstream primer 5'-CCC TAC TCG AGT TAA CCC GCG AGA CGC TGA TAT TC-3' (inserts an *XhoI* site after the end of the *yeiN* open reading frame). The purified PCR product was digested with *NdeI* and *XhoI*, purified and ligated into similarly digested pTHT, a pET-28 derived vector, which allows attachment of a modified six histidine tag followed by a tobacco etch virus protease cleavage site onto the N-terminus of the expressed protein. Colonies were screened for the presence of the insert and a representative plasmid was designated pEcYeiN.THT. The PCR-derived DNA was sequenced and shown to contain no errors.

The *yeiN* gene was further transformed into *E. coli* strain BL21(DE3) (Novagen). The cells were grown overnight in a 10 mL starter culture in Luria-Bertani (LB) media (28) containing 30 µg/mL kanamycin, then transferred to cultures containing 1.5 L LB media and incubated at 37 °C with shaking until an OD<sub>600</sub> of 0.8 was achieved. The culture was then induced with 1 mM isopropyl-1-β-D-galactopyranoside and incubated overnight at 15 °C. Cells were harvested by centrifugation at 10000 *g* for 30 min at 4 °C and resuspended in a lysis buffer containing 50 mM tris(hydroxymethyl)aminomethane (Tris), pH 8.0, 300 mM NaCl, 10 mM imidazole, and lysed by sonication. The lysate was centrifuged at 40000 *g* for 30 min and the supernatant was loaded onto a column containing 2 mL Ni-NTA resin (Qiagen) preequilibrated with the lysis buffer. The column was then washed with three times the volume of wash buffer containing 50 mM Tris, pH 8.0, 300 mM NaCl and 30 mM imidazole for 1.5 h. The protein was eluted with 50 mM Tris, pH 8.0, 300 mM NaCl, and 250 mM imidazole. The eluted protein was then subjected to size exclusion chromatography using an ACTA Explorer FPLC with a HiLoad 26/60 Superdex 200 prep grade column (GE Healthcare). The resulting protein was more than 95% pure as judged by SDS-PAGE analysis (unpublished experiments). The protein was then concentrated to 15 mg/mL using an Amicon concentrator (30 kDa MWCO filter, Millipore), flash frozen and stored at -80 °C.

### ΨMP Glycosidase Mutagenesis

Site directed mutagenesis was performed by a standard PCR protocol using *Pfu*UltraII DNA polymerase per the manufacturer's instructions (Agilent) and *DpnI* to digest the methylated parental DNA prior to transformation. In addition to the forward and reverse primers required to introduce the mutation, a third primer was designed to screen for the presence of the mutation by colony PCR (Supplementary Table 1). For screening, the primers designated "sF" were paired with the T7T primer (5'-GCTAGTTATTGCTCAGCGG-3') and the primers designated "sR" were screened with the T7Plac primer (5'-TATAGGGGAATTGTGAGCGG-3'). All the mutants were verified by sequencing.

### Enzymatic Synthesis of ΨMP

2.5 mg ΨMP glycosidase, 100 mM uracil and R5P were incubated in a buffer containing 0.5 mM MnCl<sub>2</sub>, 25 mM HEPES, pH 7.1 at 25 °C for 1 h. The enzyme was removed using an Amicon 30 kDa MWCO (Millipore) filter. The reaction product was identified as ΨMP by comigration with an authentic sample of ΨMP during HPLC analysis.

## Crystallization of ΨMP Glycosidase

ΨMP glycosidase was crystallized using the hanging drop vapor diffusion method at 22 °C. The initial crystallization condition was determined using sparse matrix screens Crystal Screen 1 and 2 (Hampton Research). The optimized reservoir conditions were 20% polyethylene glycol 4000, 0.2 M sodium acetate and 0.1 M Tris, pH 7.0. ΨMP glycosidase was incubated with 4 mM MnSO<sub>4</sub> before crystallization. The drops contained 1.5 μL of protein solution and 1.5 μL of reservoir solution. Prismatic crystals grew within 2 d to the size of 200 μm × 50 μm × 50 μm.

The ΨMP glycosidase/R5P complex was co-crystallized under similar conditions except that the protein was incubated with 4 mM MnCl<sub>2</sub> and 2 mM R5P for 30 min prior to crystallization. The ΨMP glycosidase/ ring-opened ribose ΨMP complex was obtained by co-crystallizing ΨMP glycosidase with 4 mM MnCl<sub>2</sub>, 2 mM R5P and saturated uracil. The K166A/ΨMP complex was prepared by cocrystallizing the mutant enzyme with R5P and uracil.

## Data Collection and Processing

Prior to the data collection, crystals were soaked in a cryoprotectant solution of 5% glycerol in the mother liquor to avoid damage during vitrification. Data sets for ΨMP glycosidase and the complexes were collected at the Northeast Collaborative Access Team (NE-CAT) beamline 24-ID-C at the Advanced Photon Source (APS) using an ADSC Quantum 315 detector (Area Detector Systems Corporation) at a wavelength of 0.9795 Å with 1 s exposure times and 1° oscillation angles. The detector distances were 275, 350, 325 and 200 cm for the ΨMP glycosidase, the R5P complex, the ring-opened ribose ΨMP complex and the K166A/ΨMP complex, respectively. Data were indexed, integrated and scaled using the HKL2000 program suite (29). Data collection statistics are summarized in Table 1.

## Structure Determination and Refinement

The structure of EcΨMP glycosidase was determined by molecular replacement using MOLREP (30). The search model was a monomer of PDB ID 1VKM, which has 39% sequence identity to ΨMP glycosidase, after modification by CHAINSAW (31). 1VKM was originally reported to be an indigoidine (IndA)-like protein from *Thermotoga maritima* (26), but later shown to be a ΨMP glycosidase (4). The model was refined through successive rounds of manual model building using COOT (32) and restrained refinement with REFMAC5 (33). Water molecules were then included after the model converged, followed by two additional rounds of refinement. The structure of the ΨMP glycosidase/ring-opened R5P adduct was determined by using the structure of unliganded ΨMP glycosidase as the model and refining with REFMAC5 (33). The structure of the ΨMP glycosidase/ ring-opened ribose ΨMP adduct, which crystallized in a different space group, was determined by molecular replacement using MOLREP (30) using a monomer from the refined ΨMP glycosidase as the search model. The structure of the K166A/ΨMP complex was determined by using the structure of the ΨMP glycosidase/ ring-opened ribose ΨMP adduct as the model and refining with REFMAC5 (33). The ligand contents and alternative side chain conformations were determined by F<sub>o</sub>-F<sub>c</sub> maps and composite omit maps from PHENIX (34). All ligands were clearly observed in the composite omit map, but were not placed until the last stage of the refinement. The final refinement statistics are summarized in Table 1.

## HLPC Analysis of the Reaction Mixture

HPLC analysis following a linear gradient, at a flow rate of 1 mL/min, was used with absorbance detection at 254 nm. Solvent A was water, solvent B was 100 mM K<sub>2</sub>HPO<sub>4</sub>, pH 6.6 and solvent C was methanol: 0 min, 100% B; 5 min, 10% A, 90% B; 7 min, 25% A,

60% B, 15% C; 17 min, 25% A, 60% B, 15% C; 19 min, 30% A, 40% B, 30% C; 21 min, 100% B; 30 min 100% B. The column used was a Supelcosil LC-18- T HPLC column (15 cm × 4.6 mm, 3 μM particle size).

### Time Course for the Reverse ΨMP Glycosidase Reaction

The reaction mixture contained 20 μM uracil, R5P, and 250 μM Mn(II). The reaction mixture was divided into 90 μL aliquots and 10 μL of 10 μM ΨMP glycosidase was added to achieve a final concentration of 1 μM ΨMP glycosidase. The reaction was quenched at 20 s, 40 s, 1 min, 2 min, and 5 min by heating it at 100 °C for 2 min. The samples were filtered (10 kDa MWCO) and analyzed by RP-HPLC using the method described above. The peak areas for ΨMP were integrated and plotted against time.

For the K166A mutant, the reaction mixture (1 mL) contained 500 μM each of uracil, R5P, and 250 μM of Mn(II). The reaction mixture was divided into 90 μL aliquots and 10 μL of 200 μM K166A was added to achieve the final concentration of K166A (20 μM). The reaction was quenched at 20 s, 40 s, 1 min, 2 min, 3 min, 5 min, 10 min and 20 min time points by heating each reaction mixture at 100 °C for 2 min. The reaction samples were filtered (10 kDa MWCO) and analyzed by RP-HPLC. The peak area for ΨMP was integrated and plotted against time.

### Determination of $k_{cat}$ and $K_m$ for the Reverse ΨMP Glycosidase Reaction

Uracil concentrations were varied while keeping the R5P concentration at saturation (1 mM) and the Mn(II) concentration at 250 μM. ΨMP formation was monitored by HPLC analysis. Each reaction mixture was divided into 90 μL aliquots and 10 μL of 10 μM ΨMP glycosidase was added to achieve the final concentration of 1 μM. For each set of reactions, the reaction was quenched at 20 s, 40 s, 1 min, 2 min, 3 min, 5 min, and 10 min time points by heating at 100 °C for 2 min. In the case of K166A, the uracil concentrations were varied while keeping R5P concentration at 1 mM and Mn(II) concentration at 250 μM for five different sets of reactions. Each reaction mixture was divided into 85 μL aliquots and 15 μL of 250 μM K166A was added to start the reaction (final concentration 37.5 μM). For each set of reactions, the reaction was quenched at 20 s, 40 s, 1 min, 2 min, 3 min, 5 min, and 10 min time points by heating at 100 °C for 2 min. All samples were analyzed by HPLC and the amount of ΨMP formed was plotted against time for each set of substrate concentrations. The initial slopes from each set of reactions were then plotted against the substrate concentration and fit to the Michaelis-Menten equation using KaleidaGraph (Synergy Software). The mutant E31A, K93A, H137A, D149A, and N289A activities were measured using a similar procedure.

### Biochemical Characterization of the ΨMP Glycosidase R5P Adduct

A reaction mixture containing 2 mM R5P and 1 mM Mn(II) in 50 mM Tris-HCl, 100 mM NaCl and 2 mM TCEP (pH 8.0) was incubated at room temperature for 1 h with ΨMP glycosidase (50 μM), followed by addition of sodium borohydride (2 mg) and further incubation at room temperature for 45 min. The sample was then buffer-exchanged into 10 mM ammonium acetate (pH 8.0) using a Bio-Rad desalting column and analyzed by ICR-MS. Control samples, one containing 2 mM uracil and the other lacking R5P and Mn(II) were similarly prepared and analyzed.

To locate the site of adduct formation, trypsin digestion analysis was performed on each of these samples as follows: 10 μL of guanidine-HCl (6 M) was added to each sample (50 μL containing 100 μg of ΨMP glycosidase), followed by 1 μL of DTT (200 mM). After a 1 h incubation at room temperature, 10 μL of iodoacetamide (200 mM) was added and the reaction mixture was further incubated in the dark for 1 h. 29 μL of ammonium bicarbonate

buffer were further added to reduce the final concentration of guanidine-HCl to 0.6 M (final volume 100  $\mu$ L). 1  $\mu$ L of trypsin in 50 mM ammonium bicarbonate buffer, pH 8.0 (1  $\mu$ g/ $\mu$ L) was added and the samples were incubated at 37 °C for 20 h. The samples were then analyzed by LC-MS

## RESULTS

### Overall Structure of $\Psi$ MP Glycosidase

$\Psi$ MP glycosidase is a homotrimer (Figure 1A) with one trimer per asymmetric unit in the crystal structure. Of the 312 possible residues, each protomer is complete except for the first two to five residues at the N-terminus and the C-terminal residue, which is missing in most of the protomers.  $\Psi$ MP glycosidase shows an  $\alpha\beta\alpha$  fold. The central mixed  $\beta$ -sheet contains 11 strands with topology  $1\uparrow 4\uparrow 3\downarrow 2\downarrow 7\downarrow 8\downarrow 11\downarrow 9\downarrow 10\downarrow 5\uparrow 6\uparrow$  and is flanked by six  $\alpha$ -helices on one side and seven  $\alpha$ -helices on the other (Figure 1B, C). The structure of the protomer is similar to that of PDB ID 1VKM (26), which was used as a search model during molecular replacement. The trimer contains a buried surface area of 8650  $\text{\AA}^2$ , accounting for 27.8 % of the total surface area. The trimer interface is formed primarily by helices  $\alpha 5$  and  $\alpha 8$  from one protomer and helices  $\alpha 9$  and  $\alpha 10$  from the adjacent protomer. The interface includes hydrogen bonds between Ile146-Thr180\* (\* indicates residues from an adjacent protomer) and Arg96-Asn228\*, and a salt bridge between Arg97 and Glu179\*.

### Mn(II) Binding Site

Mn(II) is required for  $\Psi$ MP glycosidase activity (4) and for the formation of high quality crystals. The Mn(II) coordination is octahedral with Mn(II) to oxygen distances ranging from 2.13  $\text{\AA}$  to 2.35  $\text{\AA}$  (Figure 2). Only one protein residue, Asp145, participates in coordination and water molecules (W1-W5) occupy the remaining five positions. The coordinating oxygen atoms interact with protein atoms, substrate atoms (see below), and other water molecules. W1 hydrogen bonds to Glu179\* and a  $\Psi$ MP phosphate oxygen atom, W2 hydrogen bonds to His137 and a  $\Psi$ MP phosphate oxygen atom, W3 hydrogen bonds to Asp145, the carbonyl oxygen atom of Gly266, W4 hydrogen bonds to Glu176\* and Glu179\*, W5 hydrogen bonds to a water molecule in the second sphere (W11) and a water molecule (W7) that bridges to the  $\Psi$ MP phosphate. The water molecules directly involved in Mn(II) interactions are involved in additional hydrogen bonding interactions that extend into the remainder of the active site.

### $\Psi$ MP Glycosidase Active Site

The active site, as defined by the structure of the K166A/ $\Psi$ MP complex, is located in a cleft formed by helices  $\alpha 12$ ,  $\alpha 13$  and the loops following strands  $\beta 2$ ,  $\beta 7$ , and  $\beta 8$  (Figure 3A, B). The  $\Psi$ MP ribose is in a C3'-endo conformation, the glycosidic torsion angle is *anti*, and the C4'-C5' bond is in *gauche*, *trans* conformation. Including the Mn(II) coordination sphere, the active site contains 19 well-ordered water molecules that are present in all three protomers.  $\Psi$ MP is surrounded by 15 of the water molecules and these mediate many of the active site contacts with the protein. One of the  $\Psi$ MP phosphate oxygen atoms forms hydrogen bonds with W1 from the Mn(II) coordination sphere, Lys93, and water molecule W11. A second phosphate oxygen atom forms hydrogen bonds with W2 from the Mn(II) coordination sphere, Ser147 and water molecule W10. The third phosphate oxygen atom forms hydrogen bonds with three water molecules (W7-W9), which interact through multiple contacts with the protein (Ser95, Thr112, Ala148NH, Asp149, and Glu179\*). The ribose O2'-hydroxyl group hydrogen bonds to Glu31, the O3'-hydroxyl group hydrogen bonds to Asp149 and the Val113 amide group, while O4' hydrogen bonds with water molecule W12, which in turn hydrogen bonds to Lys93 and W19.

The  $\Psi$ MP uracil forms no direct hydrogen bonds with protein residues; however, N1, O2, N3, and O4 form hydrogen bonds with five water molecules. One water molecule (W14) hydrogen bonds to N1 and W15 and bridges to the  $\Psi$ MP phosphate through two additional water molecules (W10 and W13). The second water molecule (W16) hydrogen bonds to O2, the side chain of Asn289, W17, and W18, which is positioned over the center of the uracil ring and hydrogen bonds to the amide nitrogen and carbonyl oxygen atoms of Gly132. The third water molecule (W15) also hydrogen bonds to O2, the amide nitrogen atom of Ala166 and W14. The fourth water molecule (W18) hydrogen bonds to N3, the carbonyl oxygen atom of Gly38, and the side chain of Asn289. The fifth water molecule (W19) hydrogen bonds to O4, the carbonyl oxygen atom of His37 and an additional water molecule (W12), which hydrogen bonds to O4' of  $\Psi$ MP and Lys93.

### Structure of $\Psi$ MP Glycosidase/Ring-opened Ribose $\Psi$ MP Adduct

The structure of  $\Psi$ MP glycosidase cocrystallized with R5P and uracil shows ring-opened ribose  $\Psi$ MP covalently attached to Lys166. Ring opening and closing is correlated with an approximately 90° rotation and a 2 Å shift of the uracil (Figure 4A, B), thus occupying a different binding site compared to the K166A/ $\Psi$ MP complex. In this binding site, O2 forms a hydrogen bond with Asn289. The ring-opened ribose retains hydrogen bonds between the 2'-hydroxyl group and Glu31, and between the 3'-hydroxyl group and Asp149; however, the hydrogen bond to O3' requires a rotation of the Glu31 carboxylate about the C $\gamma$ -C $\delta$  bond compared to the  $\Psi$ MP complex. The phosphate group maintains the same position as in the K166A/ $\Psi$ MP structure and forms hydrogen bonds with Lys93, Ser147, W1, W2, and W7-W11. The water molecules near the uracil are not well defined, possibly owing to the lower resolution (2.5 Å) of this structure.

### Structure of the $\Psi$ MP Glycosidase/R5P Adduct

Crystals of  $\Psi$ MP treated with R5P show a structure in which the R5P is in the ring-opened form and is covalently attached to Lys166 via an imine. The R5P superimposes closely with the ring-opened ribose in the  $\Psi$ MP adduct and forms hydrogen bonds between the 2-hydroxyl group and Glu31, and between the 3-hydroxyl group and Asp149 (Figure 4B, C). The phosphate binding site is essentially the same as for the previous complexes. Water molecules in the uracil binding site are less ordered and more variable from protomer to protomer compared to the K166A/ $\Psi$ MP complex.

### Detection of a Lys166 R5P Covalent Adduct by Mass Spectrometry

The mass of wild type  $\Psi$ MP glycosidase was determined to be 35,453.7 Da by ICR-MS analysis (Figure 5A). The mass of the reduced R5P complex was 35,669.7 Da corresponding to a mass increase of 216 Da. This is consistent with a doubly protonated reduced R5P-derived imine (216 Da). Adduct formation was not observed when only uracil was incubated with  $\Psi$ MP glycosidase.

The site of imine formation was identified by trypsin digestion of the reduced  $\Psi$ MP glycosidase R5P adduct (Figure 5B-E). Trypsin cleaves after lysine and arginine residues and lysine modification blocks the cleavage reaction. Trypsin digestion of the unmodified enzyme yielded the peptide GAEHTFDISADLQELANTNVTVVCAGAK (Mass = 2930.4079 Da, amino acids 139-166). For glycosidase incubated with R5P, trypsin digestion yielded the peptide GAEHTFDISADLQELANTNVTVVCAGAKSILDLGLTTEYLETFGVPLIGYQTK (Mass = 5896.8759 Da, amino acids 139-191). This demonstrates that Lys166 is the R5P modified residue. This was confirmed by similar MS analysis of the K166A mutant for which no mass increase was observed for the R5P treated sample.

## Steady State Kinetics of EcΨMP Glycosidase and its Mutants

Steady state kinetic parameters were determined by measuring the production of ΨMP during the reverse reaction while varying the uracil concentration (Supplementary Material, Figure 1A). Michaelis-Menten analysis for the native enzyme indicated a  $K_m$  value of 169.6  $\mu\text{M}$  for uracil and a  $k_{cat}$  3.74  $\text{s}^{-1}$ . This corresponds to a catalytic efficiency,  $k_{cat}/K_m$ , of  $22 \times 10^3 \text{ M}^{-1} \text{ s}^{-1}$ .

Steady state kinetic parameters were also determined for the active site mutants E31A, K93A, K166A and N289A (Table 2) (Figure 1 in Supplementary Material). The activity of D149A was below the detection limit even at an enzyme concentration as high as 100  $\mu\text{M}$ . K93A has a higher  $K_m$  value compared to wild type enzyme. E31A, K93A, K166A and N289A have significantly lower  $k_{cat}$  values, with E31A and K166A showing the largest effects.

## DISCUSSION

### Comparison with Other Protein Structures

A structural similarity search for ΨMP glycosidase was performed using the DALI (35). Not surprisingly, PDB ID 1VKM, which was used as the search model during molecular replacement, showed the highest similarity with a Z score of 42.2 (sequence identity 39%). PDB ID 1VKM was originally reported by a structural genomics group to be an indigoidine synthase (IndA)-like protein from *T. maritima* (26). Subsequent biochemical studies conclusively demonstrated that this protein is a ΨMP glycosidase (4). The structure of the EcΨMP glycosidase is trimeric. The structure of ΨMP glycosidase from *T. maritima* (TmΨMP glycosidase) is hexameric in the crystal structure; however, this hexamer is an artifact resulting from face-to-face packing of two trimers, in which pairs of N-terminal His-tags are joined by metal ions. Each of the TmΨMP glycosidase trimers is homologous to the EcΨMP glycosidase trimer, and both enzymes contain a bound Mn(II).

TmΨMP glycosidase was reported to copurify with an unknown bound ligand that resembled a ring-opened sugar phosphate (26). Motivated by our structural results, we reexamined this electron density and found that in some protomers a ring-opened R5P covalently attached to a lysine residue (equivalent to Lys166 in EcΨMP glycosidase) provided a good fit to the electron density while in others the ribose was in the ring-opened form but did not appear to be covalently attached.

### Mechanistic Implications

The mechanism of pseudouridine synthase has been extensively studied and is outlined in Figure 6 (36). The microscopic reverse of this reaction would seem to be a reasonable starting hypothesis for the reaction catalyzed by ΨMP glycosidase. In this proposal, tautomerization of ΨMP **2** to give **9** followed by C-glycosyl bond cleavage and trapping of the resulting oxocarbenium ion would give **7** and **8**. Hydrolysis of **8** and protonation of **7** would complete the reaction

Our structural studies identified four snapshots of the EcΨMP glycosidase reaction coordinate. Wild type EcΨMP showed the unliganded state, although a sulfate ion from the crystallization solutions occupied the phosphate binding site. Incubation of the K166A mutant with R5P and uracil resulted in a structure with the substrate ΨMP bound in the active site. Native EcΨMP glycosidase incubated with R5P and uracil showed an intermediate in which ring-opened ribose ΨMP is covalently attached to Lys166. Finally, EcΨMP glycosidase incubated with R5P alone resulted in a structure with ring-opened R5P attached to Lys166. The last structure is similar to that of the 1VKM complex reported to



contain an unknown ligand (26). This series of structures demonstrated that the  $\Psi$ MP glycosidase catalyzed reaction occurs by a mechanism that is significantly different from the microscopic reverse of the pseudouridine synthase mechanism.

An alternative mechanistic proposal is outlined in Figure 7. Ring opening of the  $\Psi$ MP ribose gives **10**. This reaction requires acid base catalysis. As no amino acids are apparent in the structure for this role (Figure 3), the ring opening reaction probably occurs by a water-mediated protonation/deprotonation reaction. The conformation of the C-glycosidic bond is reasonable for a concerted process (the C6-C5-C1-O4a dihedral angle is  $50^\circ$ , while the optimal angle would be  $90^\circ$ ). Related ribose ring opening reactions are catalyzed by GTP cyclohydrolase (37). Following ribose ring opening, Lys166, undergoes a conjugate addition to the C-C double bond of **10** to give **11** with the proton coming from Glu31. Subsequent cleavage of the C-C glycosidic bond by a retroaldol type reaction releases the uracil anion, which is stabilized by hydrogen bonding of N1 to the hydroxyl of Thr130 and the amide NH of Gly131 and Gly132. Surprisingly, there are no stabilizing hydrogen bonds to the C2 or C4 carbonyl oxygen atoms of uracil. Hydrolysis of imine **12** gives **13**, which will then cyclize to **3**. In addition to the structures, the covalent linkage between Lys166 and the substrate is supported by the characterization of the R5P Lys166 imine by mass spectrometry. An alternative mechanism in which Lys166 displaces the pyrimidine from the ribose, as found for example in 8-oxoguanine DNA glycosylase (38), is unlikely. Lysine 166, modeled into the structure of the enzyme  $\Psi$ MP complex, is not suitably positioned for direct base displacement and the structure of the ring-opened ribose  $\Psi$ MP complex is not consistent with this mechanism. The structure of UrdGT2, with the substrates modeled into the active site, suggests that this C-C glycosyl transferase does not use an imine intermediate (24). Our analysis suggests that  $\Psi$ MP glycosidase may use a new glycosidase mechanism.

This mechanistic proposal enables us to suggest testable functions for the active site residues. Lys166 plays a key role in facilitating the C-glycosyl bond cleavage reaction and as expected the  $k_{cat}$  value of the K166A is 2900-fold lower than wild type, with no change in  $K_m$ . It is interesting that low levels of catalytic activity are observed for this mutant, suggesting that water can replace lysine in the mutant. Glu31 is likely to be the proton source for the lysine conjugate addition reaction (**10** to **11** in Figure 7). Consistent with this role, the  $k_{cat}$  value of the E31A mutant is 7500-fold lower than wild type, with little change in  $K_m$ . Lys93 contributes one of several interactions involved in phosphate binding. The  $k_{cat}$  value of the K93A mutant is 17-fold lower than wild type, with only a modest increase in  $K_m$ . Asn289 hydrogen bonds to two water molecules that are in turn hydrogen bonded to the C2 carbonyl and to N3. These interactions stabilize negative charge on the uracil in the conversion of **11** to **12** and **4**. Consequentially, the  $k_{cat}$  value of the N289A mutant is 17-fold lower than wild type, with a small increase in  $K_m$ . Asp149 forms a hydrogen bond to the substrate C3' alcohol. We would therefore expect that the activity of D149A mutant would be comparable to wild type, which is inconsistent with our finding that it shows no detectable activity. One possibility is that the D149A mutant has misfolded; however, CD spectra of wild type and D149A are nearly identical (unpublished experiments). Another possibility is that Asp149 serves indirectly as an acid/base through a charged network.

### The Role of the Hydrated Metal Binding Site

Both Ec $\Psi$ MP glycosidase and Tm $\Psi$ MP glycosidase contain heavily hydrated, octahedrally coordinated Mn(II) ions in which the ligands are an aspartate side chain and five water molecules. In addition, the water molecules in the second sphere (W6-W9) are also present in both structures, and all side chains in the second sphere are conserved, including a Glu176 and Glu179 from the neighboring protomer. This heavily hydrated metal binding site is unusual and likely plays a role in anchoring the  $\Psi$ MP phosphate. Two phosphate oxygen

atoms form hydrogen bonds to W1 and W2, which are in the Mn(II) coordination sphere. The phosphate group also hydrogen bonds to Ser147 and Lys93, which are conserved in both structures. While the ribose and uracil both undergo movement during catalysis, the phosphate remains in the same position, with no hydrogen bonding changes. ΨMP glycosidase shows highest activities with Fe(II), Co(II) and Mn(II), while Zn(II), and to a lesser extent, Ni(II), were inhibitory (4). These observations suggest that the ionic radius of the metal ion may play a role in properly positioning the substrate.

### Role of Conformational Changes in Catalysis

Both the protein and substrate undergo conformation changes during catalysis. The uracil undergoes a 90° rotation and a 2 Å shift after ring opening and Lys166 adduct formation. In the glycosidase ΨMP complex, uracil forms no hydrogen bonds with protein atoms; however, after shifting position, uracil hydrogen bonds through O2 to Asn289, which is located at the opposite end of the active site relative to the phosphate. Repositioning of the uracil also places N1 near the amide nitrogen atoms of Gly131 and Gly132, which are absolutely conserved. Heavy reliance in the binding site on water-mediated interactions is consistent with the need for major repositioning of an intermediate during catalysis.

Comparison of the 12 protomers (three each from four structures) suggests that conformational changes in the protein are also involved in catalysis. The largest differences occur in helices α11 and α12 with RMSDs ranging from 1.5 - 7.0 Å for the pairwise comparisons. At one extreme these residues insert into the active site, acting as a gate. At the other extreme these residues are extended away from the active site making room for substrate binding. In all of the structures, these residues tend to show weaker electron density and higher B-factors. A second region of structural variation occurs in residues 130-150 (α7 and α8) and 162-200 (helix α9 and β9) with RMSDs ranging from 1.5 to 5.0 Å. This region contains 14 of 17 absolutely conserved residues. While crystal packing may also play a role in the variation among protomers, the differences are consistent with gating of the active site and positioning of catalytically important residues.

### Conclusion

The ΨMP glycosidase complexes described in this paper give four snapshots of the reaction coordinate and provide key structural insights into the enzymatic hydrolysis of C-glycosides. Most glycosidases utilize a dissociative mechanism to reversibly cleave C-N and C-O glycosidic bonds. In contrast, the structural and biochemical studies reported here demonstrate that ΨMP glycosidase utilizes a mechanism involving ribose ring opening and subsequent covalent linkage between C1' and an active site lysine, thus setting the stage for a facile C-glycosyl bond fragmentation by a novel retroaldol type mechanism.

### Supplementary Material

Refer to Web version on PubMed Central for supplementary material.

### Acknowledgments

We thank Dr. Cynthia Kinsland for cloning ΨMP glycosidase, Leslie Kinsland for assistance in preparing the manuscript, the staff of the NE-CAT at the APS and the staff of the Cornell High Energy Synchrotron Source for assistance with the data collection. We thank Drs. David Russell, Pei-Jing Pai and Nathaniel F. Zinnel of the Laboratory for Biological Mass Spectrometry at Texas A&M University for the mass spectra of the native and ribose modified native enzyme. We thank Tom Payne and Dr. Brian Crane for CD spectra of wild type ΨMP glycosidase and D149A mutant.

## ABBREVIATIONS

<b>TCEP</b>	tris(2-carboxyethyl)phosphine
<b>LB</b>	Luria-Bertani
<b>Ψ</b>	pseudouridine
<b>ΨMP</b>	pseudouridine 5'-monophosphate
<b>R5P</b>	ribose 5-phosphate
<b>RMSD</b>	root mean square deviation
<b>Tris</b>	tris(hydroxymethyl)aminomethane
<b>EcΨMP glycosidase</b>	<i>Escherichia coli</i> ΨMP glycosidase
<b>TmΨMP glycosidase</b>	<i>Thermotoga maritima</i> ΨMP glycosidase
<b>NE-CAT</b>	Northeast Collaborative Access Team
<b>APS</b>	Advanced Photon Source

## REFERENCES

- Charette M, Gray MW. Pseudouridine in RNA: What, Where, How, and Why. *IUBMB Life*. 2000; 49:341–351. [PubMed: 10902565]
- Hoang C, Ferré-D'Amaré AR. Cocystal Structure of a tRNA [Psi]55 Pseudouridine Synthase: Nucleotide Flipping by an RNA-Modifying Enzyme. *Cell*. 2001; 107:929–939. [PubMed: 11779468]
- Uliel S, Liang X.-h. Unger R, Michaeli S. Small nucleolar RNAs that guide modification in trypanosomatids: repertoire, targets, genome organisation, and unique functions. *Int. J. Parasitol.* 2004; 34:445–454. [PubMed: 15013734]
- Preumont A, Snoussi K, Stroobant V, Collet JF, Van Schaftingen E. Molecular identification of pseudouridine-metabolizing enzymes. *J. Biol. Chem.* 2008; 283:25238–25246. [PubMed: 18591240]
- Feng B, Zheng MH, Zheng YF, Lu AG, Li JW, Wang ML, Ma JJ, Xu GW, Liu BY, Zhu ZG. Normal and modified urinary nucleosides represent novel biomarkers for colorectal cancer diagnosis and surgery monitoring. *J. Gastroen. Hepatol.* 2005; 20:1913–1919.
- Bililign T, Griffith BR, Thorson JS. Structure, activity, synthesis and biosynthesis of aryl-C-glycosides. *Nat. Prod. Rep.* 2005; 22:742–760. [PubMed: 16311633]
- Gopaul DN, Meyer SL, Degano M, Sacchetti JC, Schramm VL. Inosine-uridine nucleoside hydrolase from *Crithidia fasciculata*. Genetic characterization, crystallization, and identification of histidine 241 as a catalytic site residue. *Biochemistry*. 1996; 35:5963–5970. [PubMed: 8634237]
- Duerre JA. Hydrolytic Nucleosidase Acting on *S*-Adenosylhomocysteine and on 5'-Methylthioadenosine. *J. Biol. Chem.* 1962; 237:3737–&.
- Hurwitz J, Heppel LA, Horecker BL. The Enzymatic Cleavage of Adenylic Acid to Adenine and Ribose 5-Phosphate. *J. Biol. Chem.* 1957; 226:525–540. [PubMed: 13428783]
- Pugmire MJ, Ealick SE. The crystal structure of pyrimidine nucleoside phosphorylase in a closed conformation. *Structure*. 1998; 6:1467–1479. [PubMed: 9817849]
- Flaks JG, Erwin MJ, Buchanan JM. Biosynthesis of the Purines .16. the Synthesis of Adenosine 5'-Phosphate and 5-Amino-4-Imidazolecarboxamide Ribotide by a Nucleotide Pyrophosphorylase. *J. Biol. Chem.* 1957; 228:201–213. [PubMed: 13475309]
- Olsen AS, Milman G. Chinese-Hamster Hypoxanthine-Guanine Phosphoribosyltransferase - Purification, Structural, and Catalytic Properties. *J. Biol. Chem.* 1974; 249:4030–4037. [PubMed: 4368495]

13. Short SA, Armstrong SR, Ealick SE, Porter DJT. Active site amino acids that participate in the catalytic mechanism of nucleoside 2'-deoxyribosyltransferase. *J. Biol. Chem.* 1996; 271:4978–4987. [PubMed: 8617773]
14. Fromme JC, Verdine GL. Structure of a trapped endonuclease III-DNA covalent intermediate. *EMBO. J.* 2003; 22:3461–3471. [PubMed: 12840008]
15. Lairson LL, Henrissat B, Davies GJ, Withers SG. Glycosyltransferases: structures, functions, and mechanisms. *Annu. Rev. Biochem.* 2008; 77:521–555. [PubMed: 18518825]
16. Kharel MK, Pahari P, Shepherd MD, Tibrewal N, Nybo SE, Shaaban KA, Rohr J. Angucyclines. Biosynthesis, mode-of-action, new natural products, and synthesis. *Nat. Prod. Rep.* 2012; 29:264–325. [PubMed: 22186970]
17. Nolan EM, Fischbach MA, Koglin A, Walsh CT. Biosynthetic Tailoring of Microcin E492m: Post-translational Modification Affords an Antibacterial Siderophore-Peptide Conjugate. *J. Am Chem. Soc.* 2007; 129:14336–14347. [PubMed: 17973380]
18. Fischbach MA, Lin H, Liu DR, Walsh CT. In vitro characterization of IroB, a pathogen-associated C-glycosyltransferase. *Proc. Natl. Acad. Sci. U. S. A.* 2005; 102:571–576. [PubMed: 15598734]
19. Brazier-Hicks M, Evans KM, Gershter MC, Puschmann H, Steel PG, Edwards R. The C-glycosylation of flavonoids in cereals. *J. Biol. Chem.* 2009; 284:17926–17934. [PubMed: 19411659]
20. Siitonen V, Claesson M, Patrikainen P, Aromaa M, Maentsaelae P, Schneider G, Metsae-Ketelae M. Identification of late-stage glycosylation steps in the biosynthetic pathway of the anthracycline nogalamycin. *ChemBioChem.* 2012; 13:120–128. [PubMed: 22120896]
21. Oja T, Klika KD, Appassamy L, Sinkkonen J, Mantsala P, Niemi J, Metsa-Ketela M. Biosynthetic pathway toward carbohydrate-like moieties of alnumycins contains unusual steps for C-C bond formation and cleavage. *Proc. Natl. Acad. Sci. U. S. A.* 2012; 109:6024–6029. [PubMed: 22474343]
22. Dumitru RV, Ragsdale SW. Mechanism of 4-( $\beta$ -D-Ribofuranosyl)aminobenzene 5'-Phosphate Synthase, a Key Enzyme in the Methanopterin Biosynthetic Pathway. *J. Biol. Chem.* 2004; 279:39389–39395. [PubMed: 15262968]
23. White RH. The conversion of a phenol to an aniline occurs in the biochemical formation of the 1-(4-aminophenyl)-1-deoxy-D-ribitol moiety in methanopterin. *Biochemistry.* 2011; 50:6041–6052. [PubMed: 21634403]
24. Mittler M, Bechthold A, Schulz GE. Structure and Action of the C-C Bond-forming Glycosyltransferase UrdGT2 Involved in the Biosynthesis of the Antibiotic Urdamycin. *J. Mol. Biol.* 2007; 372:67–76. [PubMed: 17640665]
25. Chang A, Singh S, Phillips GN Jr, Thorson JS. Glycosyltransferase structural biology and its role in the design of catalysts for glycosylation. *Curr.Op. BioTech.* 2011; 22:800–808.
26. Levin I, Miller MD, Schwarzenbacher R, McMullan D, Abdubek P, Ambing E, Biorac T, Cambell J, Canaves JM, Chiu HJ, Deacon AM, DiDonato M, Elsliger MA, Godzik A, Grittini C, Grzechnik SK, Hale J, Hampton E, Han GW, Haugen J, Hornsby M, Jaroszewski L, Karlak C, Klock HE, Koesema E, Kreuzsch A, Kuhn P, Lesley SA, Morse A, Moy K, Nigoghossian E, Ouyang J, Page R, Quijano K, Reyes R, Robb A, Sims E, Spraggon G, Stevens RC, van den Bedem H, Velasquez J, Vincent J, Wang X, West B, Wolf G, Xu Q, Zagnitko O, Hodgson KO, Wooley J, Wilson IA. Crystal structure of an indigoidine synthase A (IndA)-like protein (TM1464) from *Thermotoga maritima* at 1.90 Å resolution reveals a new fold. *Proteins.* 2005; 59:864–868. [PubMed: 15822122]
27. Ausubel, FM.; Brent, F. *Curr. Protoc. Mol. Biol.* John Wiley and Sons; New York: 1987.
28. Vita A, Huang CY, Magni G. Uridine phosphorylase from *Escherichia coli* B.: Kinetic studies on the mechanism of catalysis. *Arch. Biochem. Biophys.* 1983; 226:687–692. [PubMed: 6357095]
29. Otwinowski Z, Minor W. Processing of X-ray diffraction data collected in oscillation mode. *Macro. Crystallogr., Pt A.* 1997:307–326.
30. Vagin A, Teplyakov A. An approach to multi-copy search in molecular replacement. *Acta Crystallogr. Sect. D-Biol. Crystallogr.* 2000; 56:1622–1624. [PubMed: 11092928]
31. Stein N. CHAINSAW: a program for mutating pdb files used as templates in molecular replacement. *J. Appl. Cryst.* 2008; 41:641–643.

32. Emsley P, Cowtan K. Coot: model-building tools for molecular graphics. *Acta Crystallogr. D.* 2004; 60:2126–2132. [PubMed: 15572765]
33. Murshudov GN, Vagin AA, Lebedev A, Wilson KS, Dodson EJ. Efficient anisotropic refinement of macromolecular structures using FFT. *Acta Crystallogr. Sect. D-Biol. Crystallogr.* 1999; 55:247–255. [PubMed: 10089417]
34. Adams PD, Grosse-Kunstleve RW, Hung LW, Ioerger TR, McCoy AJ, Moriarty NW, Read RJ, Sacchettini JC, Sauter NK, Terwilliger TC. PHENIX: building new software for automated crystallographic structure determination. *Acta Crystallogr. Sect. D-Biol. Crystallogr.* 2002; 58:1948–1954. [PubMed: 12393927]
35. Holm L, Rosenstrom P. Dali server: conservation mapping in 3D. *Nucleic Acids Res.* 2010; 38(Suppl):W545–549. [PubMed: 20457744]
36. Miracco EJ, Mueller EG. The products of 5-fluorouridine by the action of the pseudouridine synthase TruB disfavor one mechanism and suggest another. *J. Am. Chem. Soc.* 2011; 133:11826–11829. [PubMed: 21744792]
37. Rebelo J, Auerbach G, Bader G, Bracher A, Nar H, Hosl C, Schramek N, Kaiser J, Bacher A, Huber R, Fischer M. Biosynthesis of Pteridines. Reaction Mechanism of GTP Cyclohydrolase I. *J. Mol. Biol.* 2003; 326:503–516. [PubMed: 12559918]
38. Chung SJ, Verdine GL. Structures of End Products Resulting from Lesion Processing by a DNA Glycosylase/Lyase. *Chemistry & Biology.* 2004; 11:1643–1649. [PubMed: 15610848]
39. Geoghegan KF, Dixon HB, Rosner PJ, Hoth LR, Lanzetti AJ, Borzilleri KA, Marr ES, Pezzullo LH, Martin LB, LeMotte PK, McColl AS, Kamath AV, Stroh JG. Spontaneous alpha-N-6-phosphogluconoylation of a “His tag” in *Escherichia coli*: the cause of extra mass of 258 or 178 Da in fusion proteins. *Anal. Biochem.* 1999; 267:169–184. [PubMed: 9918669]

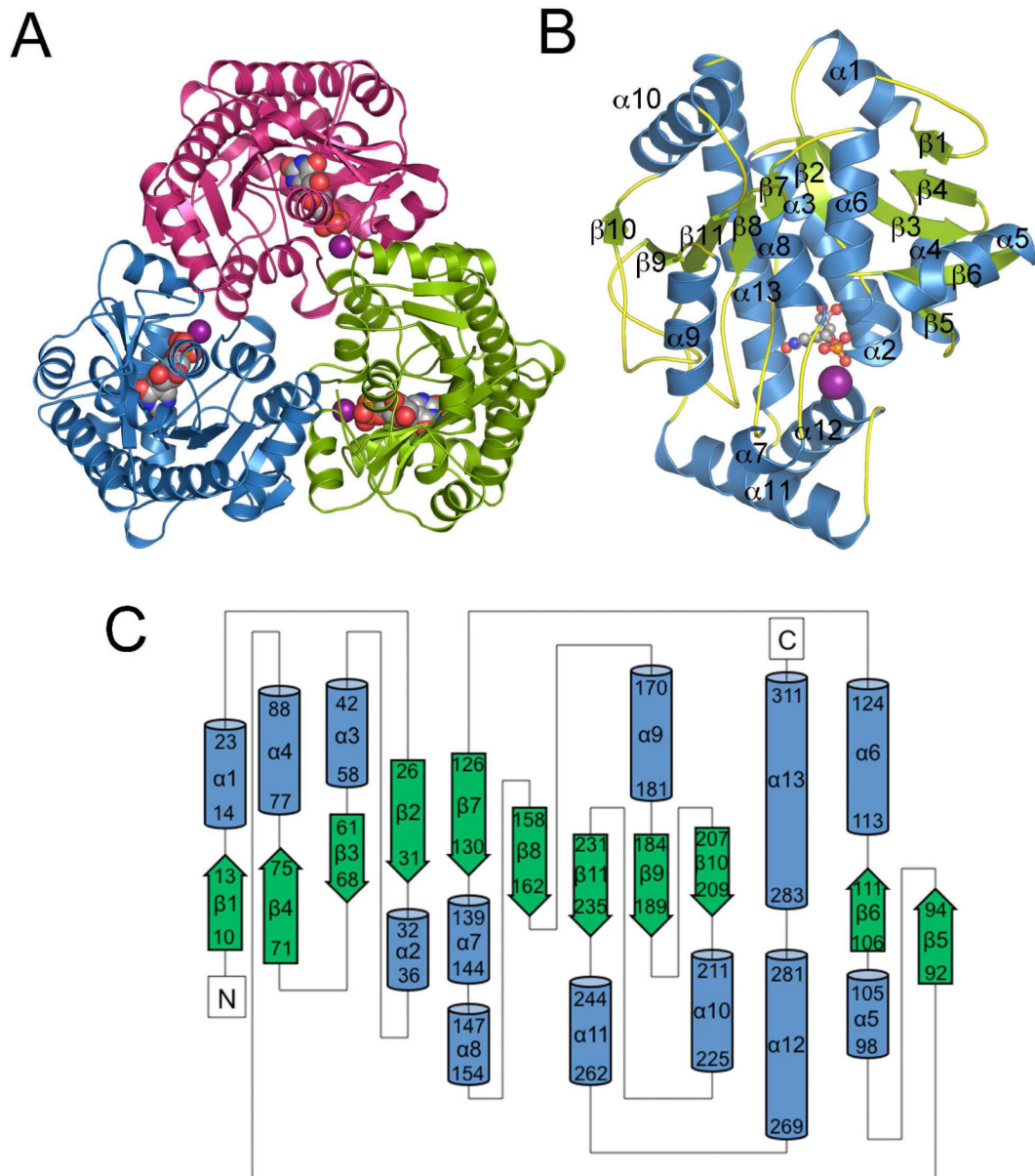


**Figure 1. Structure of ΨMP glycosidase**

(A) Ribbon diagram of the ΨMP glycosidase trimer color coded by protomer. The active site is indicated by the space filling model. The Mn(II) ion is shown in purple. (B) Ribbon diagram of a ΨMP glycosidase protomer labeled with color coded α-helices (blue) and β-strands (green). (C) Topology diagram of ΨMP glycosidase. The green arrows represent β-strands and blue cylinders α-helices. The first and last residue number of each secondary structural element is indicated.

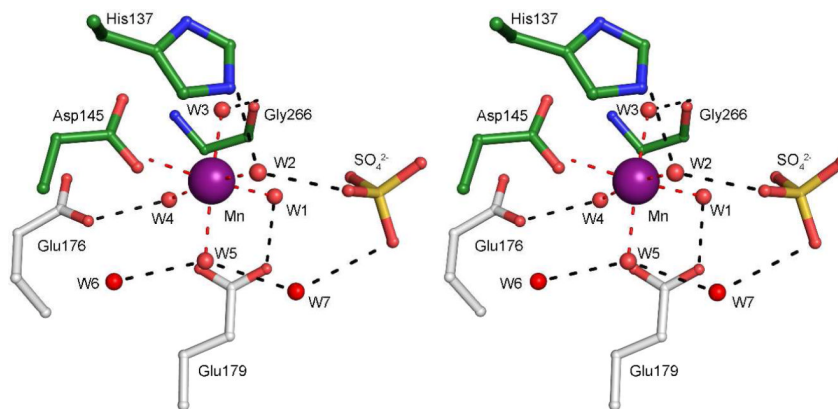


**Figure 2. Stereoview of Mn(II) binding site**  
Water molecules and protein atoms in the first and second coordination sphere are shown. The sulfate ion results from the crystallization conditions and occupies the phosphate binding site.

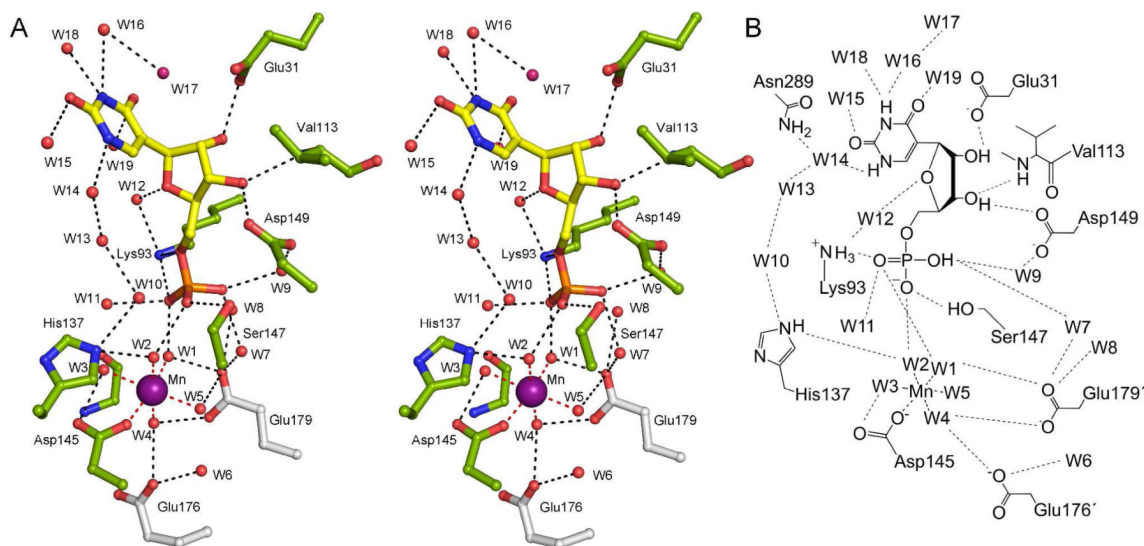


**Figure 3. ΨMP glycosidase active site**

(A) Stereoview of the K166A/ΨMP active site. ΨMP was observed in the active site when cocrystallizing K166A with either ΨMP or R5P and uracil. ΨMP and Mn(II) form extensive hydrogen bond connections with the active site residues and water molecules. The dashed lines represent interactions provided by the residues that make up the hydrogen bond network. (B) Schematic diagram of K166A/ΨMP.



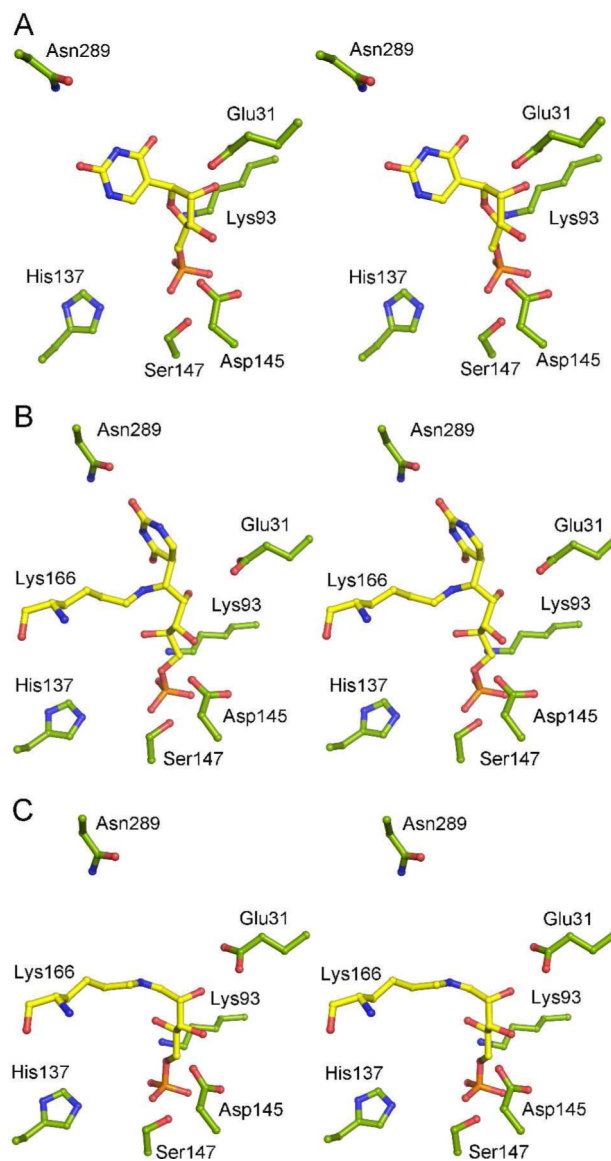


**Figure 4. Comparison of ΨMP glycosidase complexes**

(A) Stereoview of the K166A/ΨMP complex. (B) Stereoview of the ΨMP glycosidase/ring-opened ribose ΨMP adduct. (C) The ΨMP glycosidase/R5P adduct. Protein carbon atoms are shown in green; ligand carbon atoms in yellow.

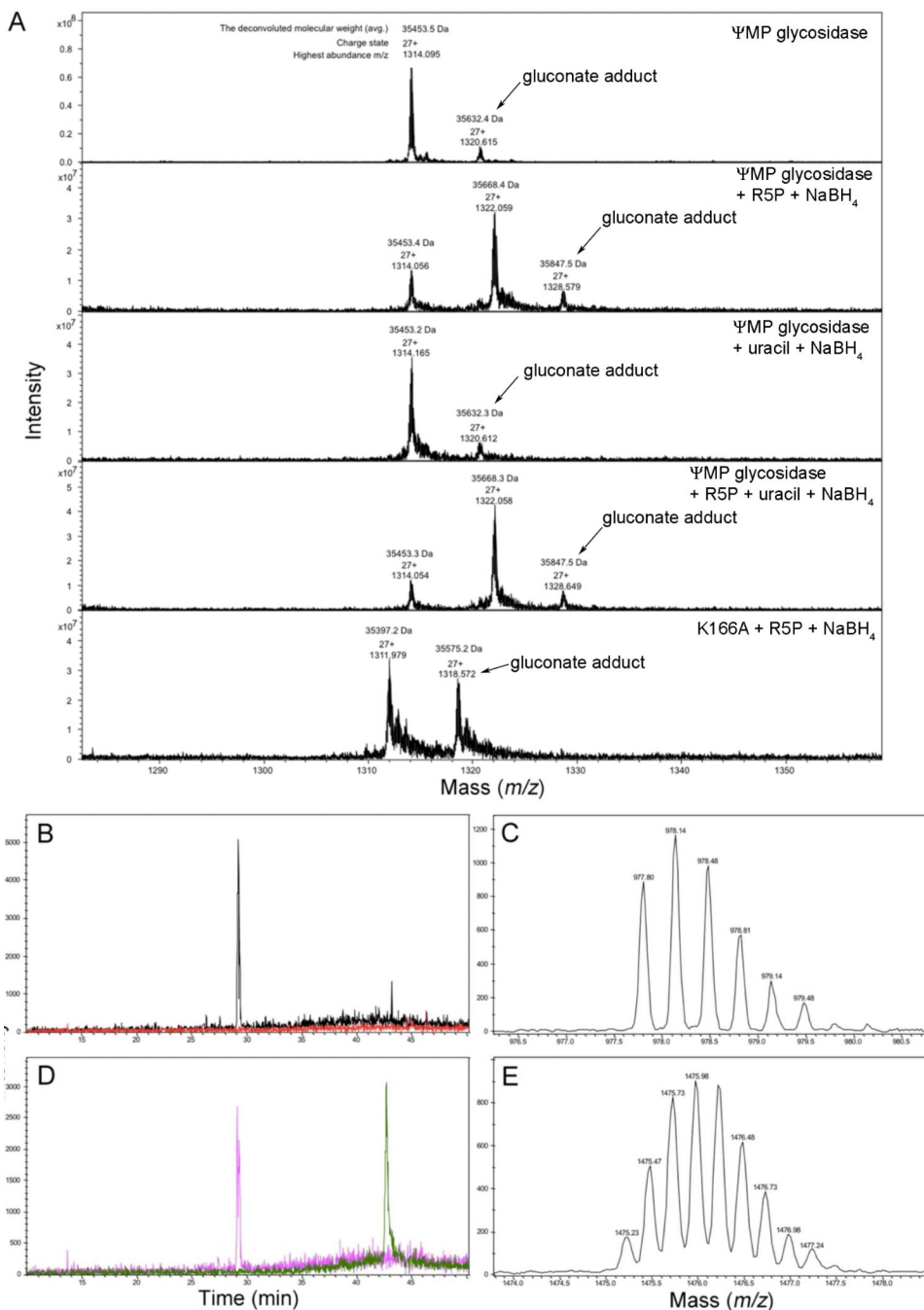


**Figure 5. Analysis of the R5P adduct by mass spectrometry**  
 (A) ICR-MS data for the identification of the borohydride reduced ΨMP glycosidase/R5P adduct. The observed 179 Da adduct corresponds to enzyme gluconoylation (39). (B) MS chromatograms of the control sample. The black trace corresponds to the unmodified peptide while the red trace refers to the R5P bound peptide, which is not seen in the ΨMP glycosidase control. (C) Triply charged state of the unmodified peptide in the control ΨMP glycosidase sample. (D) MS chromatograms of the reduced ΨMP glycosidase/R5P adduct. The pink trace corresponds to the unmodified peptide while the green trace corresponds to the R5P bound modified peptide. (E) Triply charged state of the R5P bound modified peptide in the reduced ΨMP glycosidase/R5P adduct.

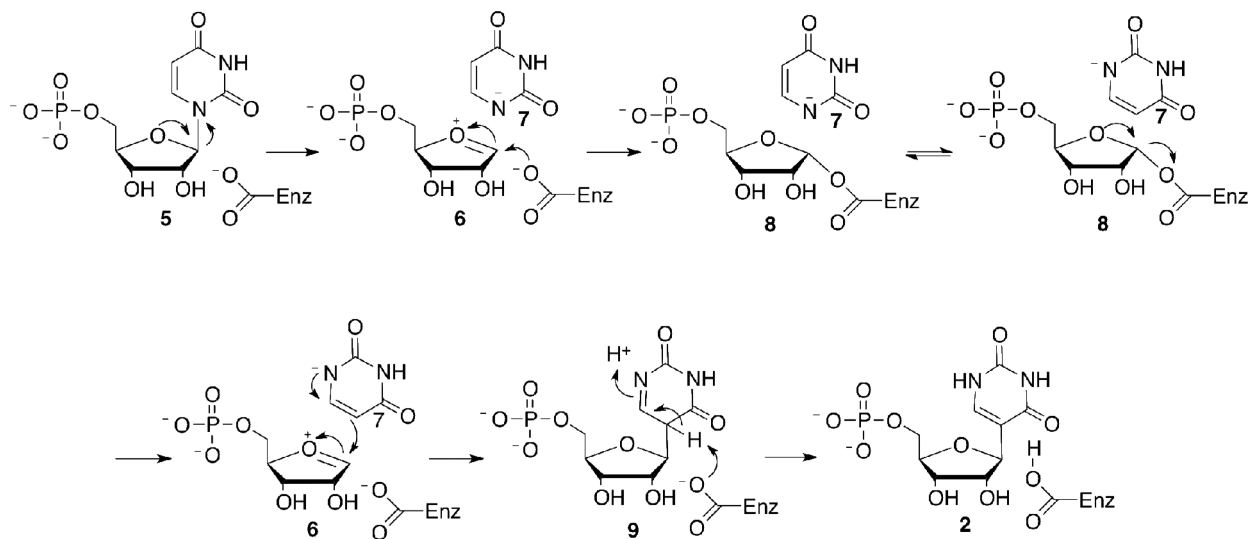


**Figure 6.** Mechanism of pseudouridine formation. This mechanism suggested a plausible starting mechanistic hypothesis for ΨMP glycosidase.

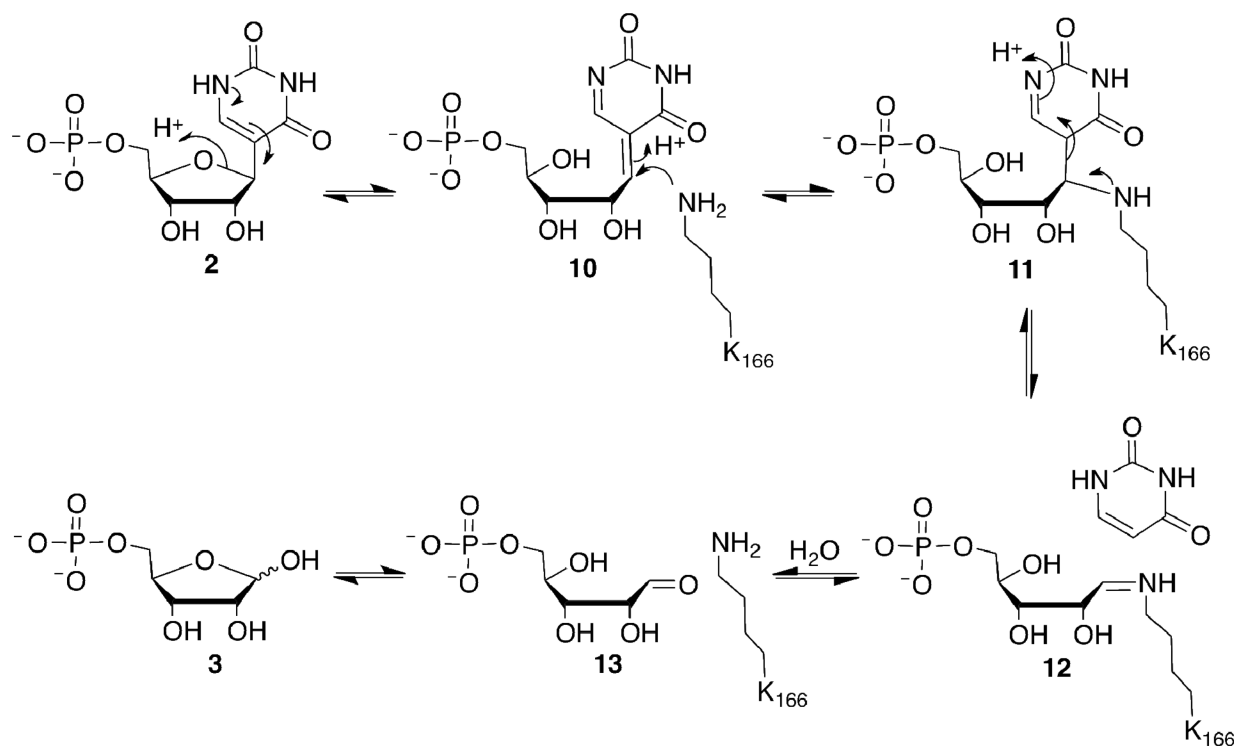
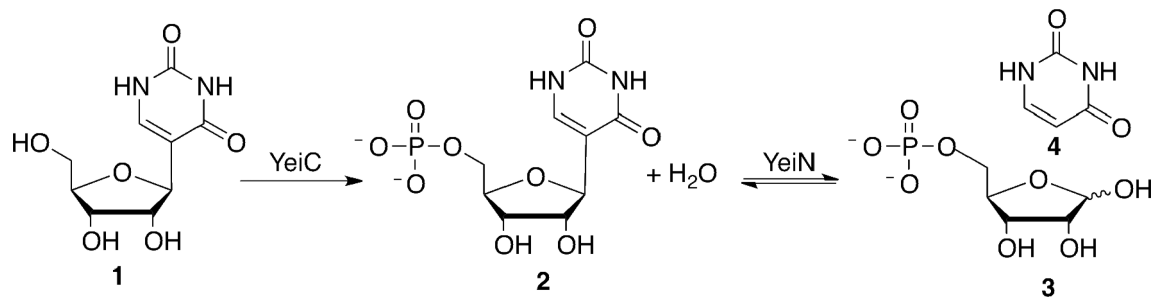


**Figure 7.**  
Mechanistic proposal for ΨMP glycosidase.



Scheme 1.

Table 1

## Data Collection and Refinement Statistics

	ΨMP glycosidase	ΨMP glycosidase / ring-opened R5P	glycosidase/ring-opened ribose ΨMP	K166A/ΨMP
beamline	APS 24-ID-C	APS 24-ID-C	APS 24-ID-C	CHESS F1
wavelength (Å)	0.9792	0.9795	0.9795	0.9180
space group	$P2_12_12_1$	$P2_12_12_1$	$P2_12_12_1$	$P2_12_12_1$
<i>a</i> (Å)	62.1	61.3	61.5	60.7
<i>b</i> (Å)	115.4	116.5	77.1	76.4
<i>c</i> (Å)	132.0	132.2	200.0	199.0
chains per asymmetric unit	3	3	3	3
resolution (Å)	43.5-2.0 (1.94-1.96) <sup>a</sup>	41.2-2.2 (2.19-2.32)	48.1-2.5 (2.50-2.57)	35.3-1.8 (1.80-1.82)
total no. of reflections	404995	196780	124598	422749
number of unique reflections	70995	49316	33815	86433
redundancy	5.7 (5.5)	4.0 (4.0)	3.7 (3.4)	4.9 (4.9)
R <sub>merge</sub> (%) <sup>b</sup>	5.5 (34.3)	6.0 (40.9)	7.5 (44.1)	7.3(43.1)
1/σ(I)	25.1 (4.2)	17.6 (2.4)	17.5 (3.1)	20.4 (3.6)
no. of reflections in working set	66972	45946	31542	81618
completeness (%)	99.7 (99.6)	99.8 (99.9)	99.1 (96.9)	99.1(100)
R <sub>work</sub> / R <sub>free</sub> (%) <sup>c</sup>	18.5/22.0	17.9/23.1	18.5/26.1	17.7/20.7
no. of protein atoms	6423	6533	6399	6575
no. of ligand atoms	18	69	93	66
no. of water atoms	375	328	210	644
average B-factor protein (Å <sup>2</sup> )	35.0	41.4	53.5	27.3
average B-factor water (Å <sup>2</sup> )	34.1	37.3	39.9	31.3
average B-factor ligand (Å <sup>2</sup> )	57.7	39.5	49.5	17.6
rmsd for bonds (Å)	0.008	0.007	0.008	0.007
rmsd for angles (°)	1.2	1.2	1.3	1.2

<sup>a</sup>Values in parentheses are for the highest resolution shell.

<sup>b</sup> $R_{\text{merge}} = \frac{\sum_i |I_i - \langle I \rangle|}{\sum \langle I \rangle}$ , where  $\langle I \rangle$  is the mean intensity of the N reflections with intensities  $I_i$  and common indices h,k,l.

<sup>c</sup> $R = \frac{\sum_{\text{hkl}} | |F_{\text{obs}}| - k |F_{\text{cal}}| |}{\sum_{\text{hkl}} |F_{\text{obs}}|}$  where  $F_{\text{obs}}$  and  $F_{\text{cal}}$  are observed and calculated structure factors.  $R_{\text{work}}$  is calculated over all reflections used in the refinement.  $R_{\text{free}}$  is calculated over a subset of reflections (5%) excluded from all stages of refinement.

**Table 2**Steady State Kinetic Parameters for ΨMP Glycosidase and Mutants<sup>a</sup>.

Enzyme	$k_{\text{cat}}$ ( $\text{s}^{-1}$ )	$K_{\text{m}}$ ( $\mu\text{M}$ )	$k_{\text{cat}}/K_{\text{m}}$ ( $\text{M}^{-1} \text{s}^{-1}$ )
ΨMP glycosidase	$3.74 \pm 0.14$	$169.6 \pm 21.6$	$(22 \pm 3.6) \times 10^3$
K166A	$0.0013 \pm 0.00005$	$162.4 \pm 23.5$	$8 \pm 1.5$
E31A	$0.0005 \pm 0.00005$	$191 \pm 39.3$	$2.6 \pm 0.8$
K93A	$0.22 \pm 0.007$	$300.5 \pm 21.8$	$(0.73 \pm 0.076) \times 10^3$
N289A	$0.23 \pm 0.007$	$214.2 \pm 18.7$	$(1.1 \pm 0.13) \times 10^3$
D149A	NA <sup>b</sup>	NA	NA

<sup>a</sup>All the kinetic parameters were determined by monitoring the conversion of uracil to ΨMP under a saturating R5P concentration;  $k_{\text{cat}}$  and  $K_{\text{m}}$  are determined for uracil.

<sup>b</sup>No activity was detected under standard assay conditions.